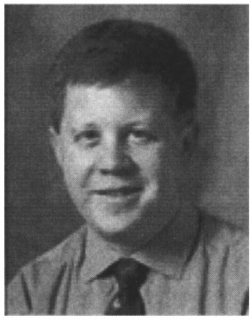

Brian E. Fischer
Integrity Applications Inc.
900 Victors Way, Suite 220
Ann Arbor, MI 48108 USA
Tel: +1 (734) 997-7436 x38
E-mail: bfischer@integrity-apps.com

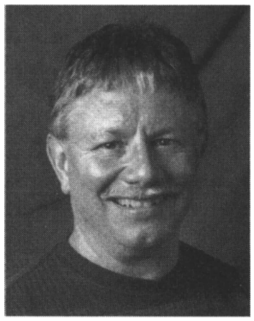

Ivan J. LaHaie
Integrity Applications Inc.
900 Victors Way, Suite 220
Ann Arbor, MI 48108 USA
Tel: +1 (734) 997-7436 x724
E-mail: ilahaie@integrity-apps.com

Introduction

The problem of detecting, locating, and tracking dismounts (moving people), using a distributed collection of simple and cheap narrowband (and, hence, low-resolution) radar devices, is an extremely challenging problem. It has been a topic of considerable research for the past several years. In particular, system performance is dependent upon both the positioning of the devices and the detection/tracking algorithms applied to the raw radar data. This month's Measurements Corner paper describes a novel Bayes-optimal nonlinear filtering technique for the latter. It demonstrates that reasonable dismount tracking can be accomplished with 5-10 m bistatic range-resolution systems.

Exploiting Narrowband Bistatic Radar Measurements for Dismount Detection and Tracking

Chris Kreucher
Integrity Applications Incorporated, Fusion Group
900 Victors Way, Suite 220, Ann Arbor MI 48108 USA
Tel: +1 (734) 997-7436 x716; E-mail: ckreucher@integrity-apps.com

Abstract

This paper describes a statistical signal-processing method for exploiting narrowband bistatic RF measurements to detect and track moving people (hereafter referred to as "dismounts"). In our approach, RF measurements are made by a constellation of narrowband radar units, arranged around a surveillance region. There are several benefits of narrowband radar in this application, which we describe in the paper. However, the narrow bandwidth means that individual measurements only yield coarse information about target state. We show that by fusing measurements from multiple bistatic sensors over time with a Bayesian nonlinear-filtering algorithm, we can effectively estimate dismount position and velocity using as little as 5-10 m bistatic range resolution. We illustrate the algorithm's efficacy with an experiment where a moving person is detected and tracked from a constellation of four narrowband bistatic sensors.

Keywords: Bistatic radar; detection and tracking; sensor fusion; nonlinear filtering; radar signal processing; density estimation

1. Introduction

This paper describes a method for detecting and tracking moving targets using measurements from a constellation of inexpensive bistatic narrowband RF sensors. Measurements are made using a commercial step-frequency radar in a cluttered environment. These measurements couple nonlinearly to the state we wish to estimate, and are corrupted by non-Gaussian noise. We present a Bayes-optimal method for fusing these measurements to effectively locate the moving target. We illustrate the efficacy of the method using bistatic measurements with 5-10 m range resolution to track a moving target.

A constellation of narrowband sensors has a number of benefits over conventional wideband sensors in this application. First, commercial applications have led to an erosion of the available spectrum, meaning often only a small portion is available for other use [1]. Furthermore, narrowband sensors are inexpensive, due to their simple electronics, require low energy consumption, are easy to maintain, and it is easy to communicate their data to a centralized processing point. However, perhaps most importantly, a constellation of narrowband sensors provides geometric diversity. By combining bistatic measurements with advanced signal-processing techniques such as those described here, this trades costly spectral diversity for cost-efficient spatial diversity, while providing performance improvement.

The main contributions of this paper are the description of a Bayes-optimal nonlinear-filtering method, which admits nonlinear and non-Gaussian measurements made by the sensors, and a validation of its assumptions using measurements from a four-antenna bistatic radar setup.

Standard methods [2] address the tracking problem in two sequential phases: detection and tracking. In particular, one algorithm is responsible for generating threshold exceedances (detections) at each epoch. These detections are then passed to a separate (typically, Kalman-based) tracking algorithm. In contrast, our approach performs track-before-detect and fuse-before-track, i.e., there is no thresholding (or other hard decision) on received measurements, and all measurements are incorporated softly into a probabilistic estimate. Furthermore, our method directly models non-Gaussian measurement statistics, such as those received after signal processing, which generates a pixilated data cube. Finally, the nonlinear-filtering method also directly models indirect nonlinear measurements of the quantities of interest.

This problem has received some attention in the literature. Of particular relevance is [3], which recently appeared in this column. In that interesting work, a collection of wideband radars made measurements of a dismount in a see-through-the-walls application. In contrast, the work we report on here uses narrowband measurements, and employs a tracker to synthesize measurements over time. Multi-static range and range-rate tracking have also received some attention. References [4-6] approached the problem using a direct-measurement model with Gaussian error, rather than the pixilated Rayleigh model we use here. References [5, 6] used extended Kalman-filter-type approaches, rather than the nonlinear-filtering approach we use. Reference [7] treated the problem with a nonlinear-filtering approach, but in an active-sonar setting, which required a very different physical model.

The paper proceeds as follows. Section 2 describes a statistical model for the measurements. Section 3 briefly describes how the model is combined with a nonlinear filter to provide a tractable Bayes optimal estimation. Section 4 describes an experiment where we collected narrowband bistatic range and range-rate measurements from a four-antenna constellation, and validated the tracking algorithm and modeling approach. Finally, Section 5 provides some concluding remarks.

2. The Sensor Model

We assume a constellation of N sensors. To simplify the notation, we assume each sensor is both a transmitter and a receiver, although this assumption is not a requirement. A sensor transmits a narrowband RF signal, which is reflected off the target and received at each sensor. This process repeats $N-1$ times, with each sensor serving as transmitter. There are then N^2 bistatic pairs, which use Fourier processing on the received data to generate a bistatic-range/bistatic-range-rate surface [8]. This surface is nonlinearly related to the state of the target, and is corrupted by various types of noise. The aim of this section is to describe a physics-based statistical model of the observables.

Let z_{ij} denote the envelope-detected value in the $(i,j)th$ bistatic range/range-rate resolution cell. The number of cells and the cell resolution are determined by the number of pulses, the pulse-repetition frequency (PRF), the coherent processing interval (CPI), and the bandwidth (BW) of the radar [9]. The collection of measurements is then the matrix of bistatic range/range-rate correlations in each cell, i.e.,

$$z(t,r)=\begin{bmatrix} z_{11}(t,r) & \cdots & z_{1Nd}(t,r) \\ & \cdots & \\ z_{Nr1}(t,r) & \cdots & z_{NrNd}(t,r) \end{bmatrix}, \qquad (1)$$

where N_r and N_d are the number of bistatic range and range-rate cells. Figure 1 shows an example processed measurement for a 0.5 s coherent processing interval.

Let the vector $x=[x \;\; \dot{x} \;\; y \;\; \dot{y}]$ describe the true two-dimensional position and velocity of the target. The distinction between scalar x and vector x will be clear by context. The statistics of the measurement in bistatic range/range-rate cell (i,j) depend on its proximity to the true bistatic range and range-rate of

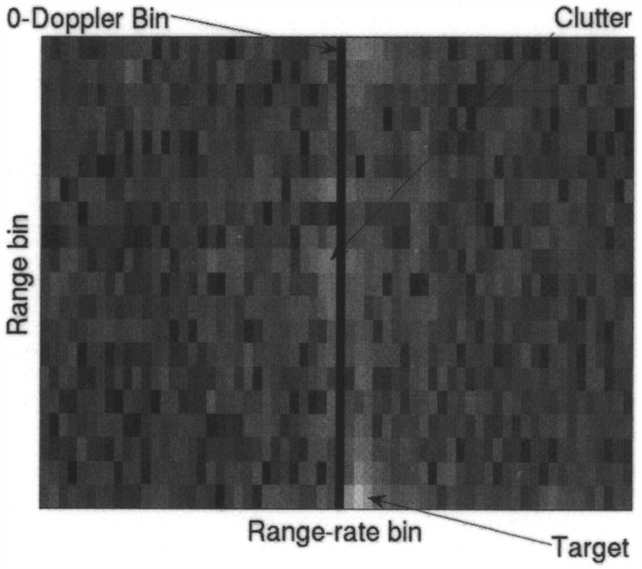

Figure 1. An example the collected range/range-rate surface.

the target. Other factors, such as the range to the target, the illumination, and the receiving pattern of the antenna may also play a role. However, these are not important in our experiments, which use a close-in target with large-beamwidth antennas, so these effects are not modeled here.

The location of the transmitter, t, will be denoted (t_x, t_y), and the location of receiver r will be denoted (r_x, r_y). With this notation, the true bistatic range and range-rate is computed as

$$R(x,t,r) = \sqrt{(x-r_x)^2 + (y-r_y)^2} + \sqrt{(x-t_x)^2 + (y-t_y)^2} \quad (2)$$

and

$$\dot{R}(x,t,r) = \frac{\dot{x}(x-r_x) + \dot{y}(y-r_y)}{\sqrt{(x-r_x)^2 + (y-r_y)^2}} + \frac{\dot{x}(x-t_x) + \dot{y}(y-t_y)}{\sqrt{(x-t_x)^2 + (y-t_y)^2}}. \quad (3)$$

This true bistatic range/range-rate maps to a particular cell, which we will denote $\hat{i}(t,r), \hat{j}(t,r)$. We use a point-target model, which ignores extended target effects such as sidelobes, the range-rate smearing that will happen in applications with a long coherent processing interval, and range extent that will happen with fine range resolution (high bandwidth). Since our application uses a short coherent processing interval and a small bandwidth, the point-target assumption is approximately valid. The extension to non-point-target models is straightforward, but is not necessary in this application.

The physical model we employ says the statistics of the target cell are Rayleigh with a target parameter, and the statistics of the background cells are Rayleigh with a background parameter:

$$p[z_{ij}(t,r)\,|\,x] = \begin{cases} 2\dfrac{z_{ij}(t,r)}{\lambda_t^2}\exp\left[-\dfrac{z_{ij}^2(t,r)}{\lambda_t^2}\right] & i,j = \hat{i}(t,r), \hat{j}(t,r) \\ 2\dfrac{z_{ij}(t,r)}{\lambda_b^2}\exp\left[-\dfrac{z_{ij}^2(t,r)}{\lambda_b^2}\right] & i,j \neq \hat{i}(t,r), \hat{j}(t,r) \end{cases} \quad (4)$$

In general, we allow the background and target mode parameters to vary with t and r, but for the sake of notational clarity we show them fixed here. Continuing with the point-target model – which assumes that measurements in different pixels are independent – we write

$$p[z(t,r)\,|\,x] = \prod_{i=1}^{Nr}\prod_{j=1}^{Nd} p[z_{ij}(t,r)\,|\,x], \quad (5)$$

and simplify successively as

$$p[z(t,r)\,|\,x] = p\left[z_{\hat{i}(t,r),\hat{j}(t,r)}(t,r)\,|\,x\right] \prod_{\substack{i=1\ j=1 \\ i,j\neq\hat{i}(t,r),\hat{j}(t,r)}}^{Nr\ Nd} p[z_{ij}(t,r)\,|\,x] \quad (6)$$

$$p[z(t,r)\,|\,x] \propto \frac{\lambda_b}{\lambda_t}\exp\left[\frac{(\lambda_t^2 - \lambda_b^2)}{\lambda_b^2\lambda_t^2} z^2_{\hat{i}(t,r),\hat{j}(t,r)}(t,r)\right] \quad (7)$$

as the probability of an $N_r \times N_d$ range/range-rate surface given the true state, x. We further assume range/range-rate surfaces are conditionally independent across transmitted/received pairs. We write the probability of all of the bistatic range/range-rate measurements from a constellation of transmitting/receiving antennas as

$$p(z\,|\,x) = \prod_t\prod_r p[z(t,r)\,|\,x] \propto \prod_t\prod_r \frac{\lambda_b}{\lambda_t}\exp\left[\frac{(\lambda_t^2 - \lambda_b^2)}{\lambda_b^2\lambda_t^2} z^2_{\hat{i}(t,r),\hat{j}(t,r)}(t,r)\right] \quad (8)$$

3. Bayesian Target Detection and Tracking

This section describes a Bayes-optimal single-target tracking algorithm that employs the model from Section 2 to fuse measurements over bistatic pair and time.

3.1 Notation

Denote the state of a target at time k as x^k, which for this work refers to the two-dimensional position and velocity, i.e., $x^k = [x \;\; \dot{x} \;\; y \;\; \dot{y}]$. Additionally, let H_0^k denote the hypothesis that no target is present at time k, and let H_1^k denote the hypothesis that a target is present. Measurements will continue to be described as follows:

- The envelope-detected value in range/range-rate cell (i,j) at coherent processing interval k from transmitter t and receiver r is denoted $z_{ij}^k(t,r)$;
- The collection of all $z_{ij}^k(t,r)$ made at a particular coherent processing interval is denoted $z^k(t,r)$, i.e., $z^k(t,r) = \left\{z_{11}^k(t,r), \cdots, z_{NrNd}^k(t,r)\right\}$;
- The collection of all measurements made at a particular coherent processing interval k (i.e., from all transmitting/receiving pairs) is denoted simply z^k, i.e., $z^k = \left\{z^k(1,1), \ldots, z^k(T,R)\right\}$;
- Finally, Z^k will denote the collection of all measurements received up to and including time k, i.e., $Z^k = \left\{z^1, \cdots, z^k\right\}$.

3.2 Approach

The Bayesian method is to estimate the joint probability a target is present (H_1^k is true) at each state x^k given the measurements. Mathematically, we estimate the hybrid continuous-discrete probability density function (PDF)

$$p\left(x^k, H_1^k \mid Z^k\right) \tag{9}$$

for all x^k, as well as the discrete probability

$$p\left(H_0^k \mid Z^k\right) = 1 - \int p\left(x^k, H_1^k \mid Z^k\right) dx^k. \tag{10}$$

Notice that we can write

$$p\left(x^k, H_1^k \mid Z^k\right) = p\left(H_1^k \mid Z^k\right) p\left(x^k \mid H_1^k, Z^k\right), \tag{11}$$

i.e., the density is the product of the *target-present probability*, $p\left(H_1^k \mid Z^k\right)$, and the *target-state probability*, $p\left(x^k, H_1^k \mid Z^k\right)$. Both conceptually and from an implementation standpoint, we treat the problem as separate (but coupled) tasks of estimating the target-present probability and estimating the target-state probability.

In the Bayesian approach, we assume that a prior estimate of the desired probabilities is present, and generate a recursion relating probabilities at one time step with those at the next. This is done in two steps, analogous to the Kalman Filter (but this is not a Kalman Filter): the temporal update, which predicts the probability distribution at time k from that at time $k-1$, and the measurement update, which corrects the predicted probability distribution at time k given the measurements received at time k.

The first step in recursive Bayesian filtering is to predict the relevant probability distributions forward in time, using statistical models based on target kinematics. The temporal update of the target present density is

$$p\left(H_1^k \mid Z^{k-1}\right) = \sum_{i=0}^{1} p\left(H_1^k \mid Z^{k-1}, H_i^{k-1}\right) p\left(H_1^k \mid Z^{k-1}\right), \tag{12}$$

where the quantity $p\left(H_1^k \mid Z^{k-1}, H_i^{k-1}\right)$ is a statistical model to be specified by studying the target-arrival properties.

Similarly, the time-predicted target-state density is based on a model of how targets move:

$$p\left(x^k \mid H_1^k, Z^{k-1}\right) = \frac{p\left(H_1^{k-1} \mid Z^{k-1}\right)}{p\left(H_1^k \mid Z^{k-1}\right)} \int p\left(x^k, H_1^k \mid x^{k-1}, H_1^{k-1}\right) p\left(x^{k-1} \mid H_1^{k-1}, Z^{k-1}\right) dx^{k-1} \tag{13}$$

where the density $p\left(x^k, H_1^k \mid x^{k-1}, H_1^{k-1}\right)$ is a statistical model of target kinematics to be specified in the particular implementation. The integral is to be interpreted as performing the multidimensional integral required. The normalizing term does not need to be evaluated, as the density can be forced to integrate to one. In this work, we assume the nearly constant velocity (NCV) model for the target. Other models, or even multiple models, are admissible under the Bayesian framework [10].

3.3 Measurement Update

The second step in Bayesian filtering is to accommodate measurements into the probability estimate. The measured data comes into the picture through the sensor model, $p\left(z^k \mid H_1^k, x^k\right)$, where the functional form of the model is specified by sensor physics, as in Section 2.

The target-present and target-absent probabilities are measurement-updated using the law of total probability and the Bayes rule, yielding

$$p\left(H_0^k \mid Z^k\right) = \frac{p\left(H_0^k \mid Z^{k-1}\right)}{p\left(z^k \mid Z^{k-1}\right)} p\left(z^k \mid H_0^k\right), \tag{14}$$

$$p\left(H_1^k \mid Z^k\right) = \frac{p\left(H_1^k \mid Z^{k-1}\right)}{p\left(z^k \mid Z^{k-1}\right)} \int p\left(z^k \mid H_1^k, x^k\right) p\left(x^k \mid H_1^k, Z_1^k\right) dx^k. \tag{15}$$

These equations expresses the current target-present and target-absent hypothesis probabilities in terms of the target-present, target-absent, and target-state probabilities predicted from the previous time step, and the conditional likelihood of incoming measurements. The normalization constant does not need to be computed, since $p\left(H_1^k \mid Z^k\right) + p\left(H_0^k \mid Z^k\right) = 1$.

The target-state probability is updated similarly:

$$p\left(x^k \mid H_1^k, Z^k\right) = p\left(x^k \mid H_1^k, Z^{k-1}\right) \frac{p\left(z^k \mid x^k, H_1^k\right)}{p\left(z^k \mid H_1^k, Z^{k-1}\right)}. \tag{16}$$

Again, constants independent of x^k are not computed.

In our application, which exploits bistatic pixilated range/range-rate measurements, the model developed in Section 2, Equation (8), provides $p\left(z^k \mid x^k, H_1^k\right)$.

3.4 Implementation

If the probability density of interest is well approximated by a Gaussian or sum-of-Gaussians, techniques such as the Extended Kalman Filter or Gaussian Sum Filter are preferred. However, in the bistatic RF case we study here, where we make measurements of bistatic range and range-rate, the density is poorly approximated by such parameterizations. We instead rely on a discrete-grid approximation to the probability density.

The details of the discrete-grid implementation are briefly reviewed here. For more detail, see [10, 11].

3.4.1 Density Representation

The PDF of x is discretized onto a four-dimensional grid (corresponding to the four-dimensional state vector, x^k) of $N_x \times N_{\dot{x}} \times N_y \times N_{\dot{y}}$ cells. The spatial extent of this grid dictates the overall region where targets may be detected. This approximation is appropriate here, given that we wish to perform surveillance over a region of fixed spatial extent.

3.4.2 Kinematic and Measurement Updates

The temporal evolution of the probability density on x^k can be expressed in continuous time using a partial differential equation. For dismount tracking, the so-called nearly constant velocity model (NCV) is appropriate, and leads to the Fokker-Plank Equation [2]:

$$\frac{\partial p}{\partial t} = -\dot{x}\frac{\partial p}{\partial x} - \dot{y}\frac{\partial p}{\partial y} + \frac{\sigma_{\dot{x}}^2}{2}\frac{\partial^2 p}{\partial \dot{x}^2} + \frac{\sigma_{\dot{y}}^2}{2}\frac{\partial^2 p}{\partial \dot{y}^2}. \quad (17)$$

Computationally, the state probability is discretized onto the grid and the update is computed from time $k-1$ to k using a backward Euler method. This approach has nice stability properties in both Δt and Δx. We use Thomas' algorithm as a fast tridiagonal solver, leading to computation that is linear in the number of grid cells. For more details, see [12]. The temporal evolution of the target-present probability assumes constant target arrival/removal.

New measurements are incorporated by updating the time-predicted grid approximation using the likelihood of the measurements. Practically, the discrete-grid probability is updated simply by point-wise multiplication of each cell in the discrete representation by the corresponding data likelihood.

4. Experimental Results

This section describes a set of measurements to validate the nonlinear-filtering algorithm described in Section 3. The experiment consists of a set of four geometrically diverse antennas that measure information about bistatic range and range-rate of a moving dismount. We show with this experimental data that our algorithm is able to accurately detect and track the dismount as it moves though the surveillance region using just 60 MHz of bandwidth (5 m bistatic range resolution).

4.1 Test Hardware

The experiment we describe here employed a commercially available AKELA AVMU500A radar, along with four SAS-510-4 antennas. The antennas were directional, and were specified to have a 3 dB point of 41° by the manufacturer. The system was selected because its size and versatility demonstrated the ability of a compact, contained system to effectively collect the necessary data.

The radar was a stepped-CW type, capable of transmitting pulses between 300 MHz and 3 GHz. The rate at which the individual frequencies were sampled was selectable, but was typically set at 45 kHz, which was the maximum rate where good data was collected. The radar had four ports, any of which could be used for transmitting or receiving. However, because the radar had only one transmitter and receiver, it was not possible to simultaneously receive multiple ports. Therefore, the collections were transmitted and received between one pair, and then moved to transmit and receive to the next pair, and so on. Since this happened at a very fast rate compared to the dismount speed, the measurements were well approximated as being simultaneous.

Figures 2 and 3 show one of the antennas as deployed, and the AKELA unit.

4.2 Experimental Setup

Four antennas (numbered 1, 2, 3, and 4) were arranged along a 35 m line and pointed toward the interior of the surveillance region, as illustrated in Figure 4. GPS measurements of the antenna locations were made with a hand-held unit, but there may have been an error of as much as 25 cm in placing the GPS units. GPS measurements were not differentially corrected. This error was not ideal, but not significant compared to the 5 m to 10 m bistatic range resolution of the measurements.

Figure 5 shows the surveillance region. The four antennas were located at $y = 0$ and $x = 0$, 13, 22, and 36 m. The antennas were pointed at the scene's center (indicated by a green circle).

4.3 Collected Data

A dismount walked a zigzag pattern in the surveillance region. Bistatic measurements were collected using Antenna 1 as the transmitter, and the other antennas (2, 3, and 4) as receivers.

In this stepped-chirp single-radar multiple-antenna system, the collection proceeded as follows: First, Antenna 1 transmitted a short pulse at the lowest frequency (1.925 GHz). Returns were received by Antenna 2. Antenna 1 transmitted a short pulse at the second-lowest frequency (1.928 GHz), which was received by Antenna 2, and so on, until the highest frequency (2.075 GHz) was completed. Once the final pulse between Antenna 1 and Antenna 2 was completed, the process was repeated between Antenna 1 and Antenna 3, and then between Antenna 1 and Antenna 4. The individual sweep pulses proceeded at 45 kHz, but the overall rate was dictated by the number of sweep pulses per pair (here chosen to be 50), the number of bistatic pairs (here there were three pairs), and the switching times. In this experiment, the actual complete-cycle pulse-repetition frequency (measured between the time the first sweep pulse was transmitted between Antenna 1 and Antenna 2 and then repeated again) was 140 Hz.

Measurements were made on the moving dismount over about a 60 s period. The true path was determined with a handheld GPS unit, which was not differentially corrected. Figure 6 shows an image of the dismount walking during the experiment.

We chose to collect data with 150 MHz of bandwidth centered around 2 GHz, with 50 sample frequencies (i.e., pulses spaced 3 MHz in frequency). This bandwidth implied a bistatic

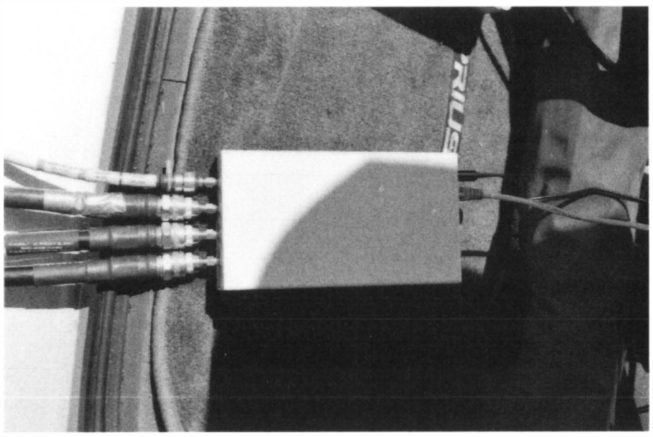

Figure 2. The Akela unit.

Figure 3. A Yagi log-periodic antenna, as deployed.

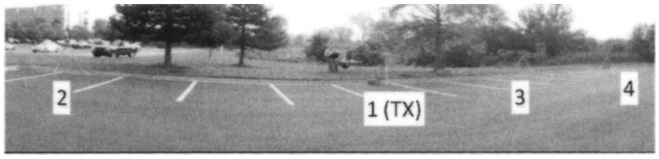

Figure 4. The four-antenna configuration used in this experiment.

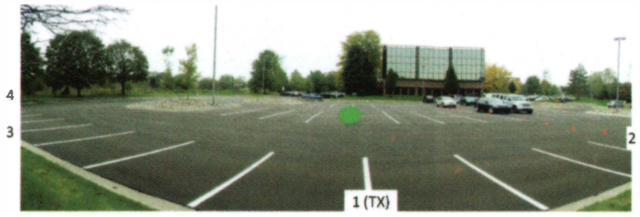

Figure 5. The surveillance region. All antennas pointed at the scene's center (denoted by the green circle).

Figure 6. An image of the dismount walking during the experiment.

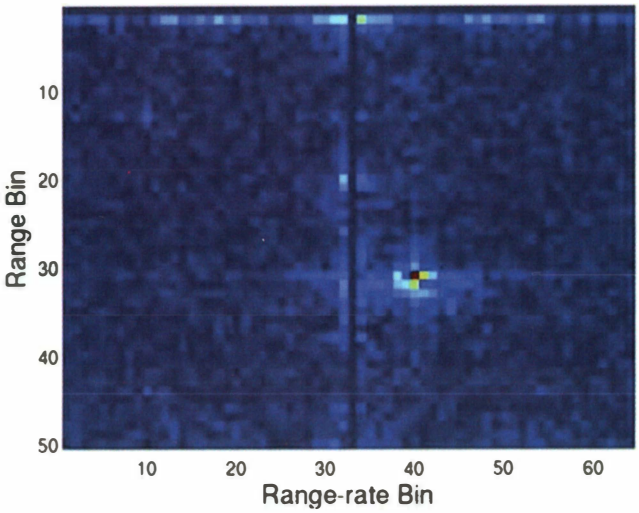

Figure 7. An example of the collected range/range-rate surface from Transmitter 1 to Receiver 3. The dismount is at range bin 30.

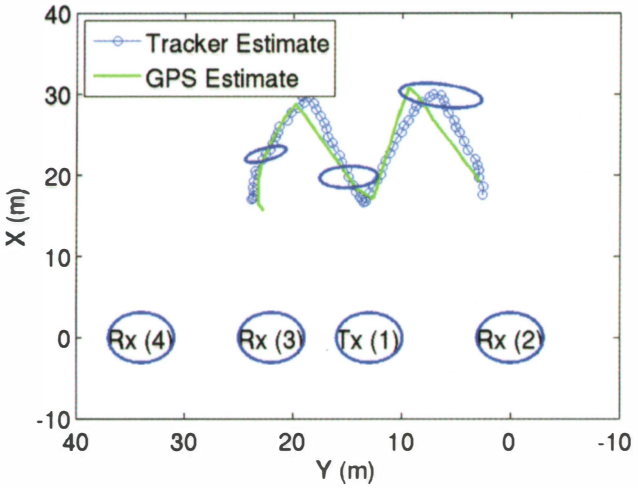

Figure 8. The tracker estimate of the dismount's position with 2 m of bistatic range resolution (150 MHz bandwidth), as compared to the GPS estimate. Tracker covariance ellipses are shown at three points during the collection for reference.

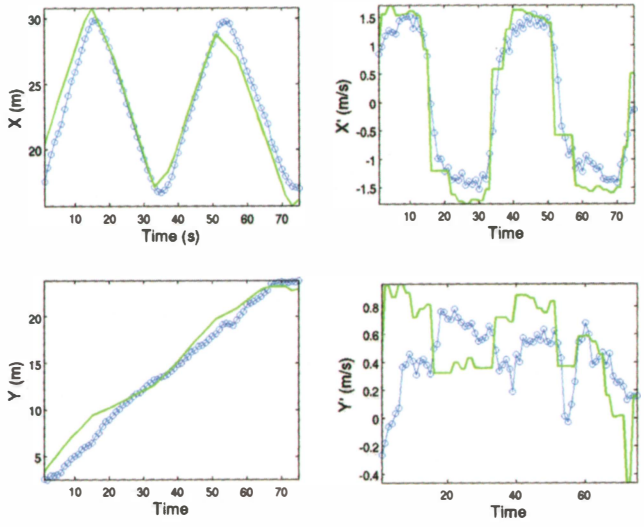

Figure 9. The tracker estimate of the dismount's position as compared to the GPS estimate of position and velocity.

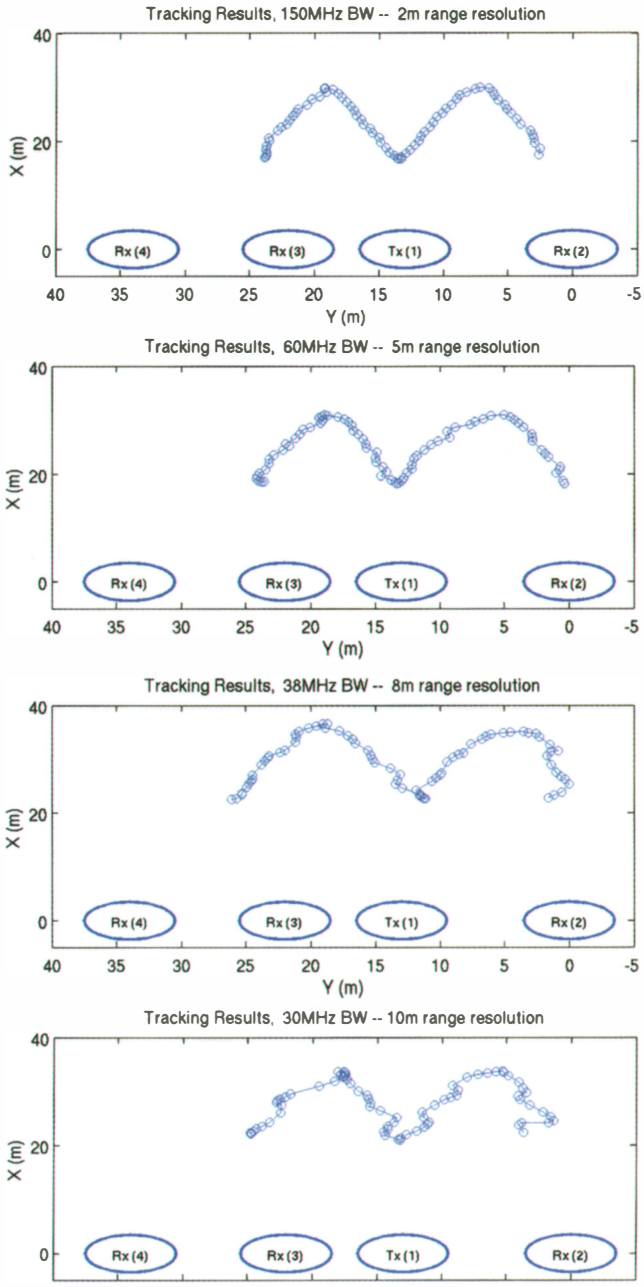

Figure 10. The tracker estimate of the dismount's position as the bandwidth was reduced.

range resolution of $c/BW = 2\,\text{m}$. In the results section, we show that we could decimate the collected data (by simply discarding data) to a bandwidth of as little as 30 MHz (10 m bistatic range resolution) and still perform credible tracking.

The received complex-frequency returns were blocked up into a 0.5 s coherent processing interval, and Fourier transformed into a range/range-rate surface, as described in Section 2. The resulting input-data surface at 150 MHz of bandwidth had 50 range bins with 2 m resolution. An example collected during this experiment is shown in Figure 7.

4.4 Results

We employed the nonlinear-filter-based target tracker described in Section 2 above. We used a $51\times31\times51\times31$ grid, and a 35 m × 6 m/s × 35 m × 6 m/s surveillance region. Tracking results using 2 m of range resolution are illustrated in Figure 8 and Figure 9. Figure 8 shows the tracker point estimate and selected covariance ellipses with respect to the GPS recordings on an xy map. Figure 9 shows the individual state-component estimates (position and velocity) as compared to the GPS estimates. Note that the GPS measurements were not differentially corrected, so there is some error in the estimate of path truth and in the transmitter/receiver locations.

We systematically reduced the bandwidth of the collected data by discarding measurements. This showed the utility of the tracking approach as the bandwidth was reduced. Figure 10 shows the tracker estimate of the target's state as the bandwidth was reduced from 150 MHz to 30 MHz (and the bistatic range resolution was changed from 2 m to 10 m).

5. Conclusion

This paper has presented a statistical signal-processing method for using RF measurements to detect and track moving targets from a narrowband constellation. Using a set of measurements, we have shown that the algorithm is able to detect and track a dismount with on the order of a range resolution of 5 m. The nonlinear-filtering approach optimally fuses bistatic range and range-rate measurements made by a collection of sensors without thresholding or linear/Gaussian assumptions, thereby improving the detection/false-alarm tradeoff, and lowering tracking error over conventional methods.

6. Acknowledgements

This work was supported by Air Force Research Laboratory contracts FA8650-09-M-1549 and FA8650-10-C-1718. The author would like to gratefully acknowledge the assistance of Ben Hart, Chris Roussi, Joe Burns, and Mike Brennan, who assisted with the collection of the experimental data used to validate this approach.

7. References

1. B. Himed, H. Bascom, J. Clancy and M. Wicks, "Tomography of Moving Targets," *Proceedings of SPIE*, **4540**, 2001, pp. 608-619.

2. Y. Bar-Shalom, X. Li, and T. Kirubarajan, *Estimation with Applications to Tracking and Navigation*, New York, John Wiley and Sons, 2001.

3. A. Schmitt and P. Collins, "Demonstration of a Network of Simultaneously Operating Digital Noise Radars," *IEEE Antennas and Propagation Magazine*, **51**, 2, 2009, pp. 125-130.

4. M. Tobias and A. Lanterman, "Probability Hypothesis Density-Based Multitarget Tracking with Bistatic Range and Doppler Observations," *IEE Proceedings Radar, Sonar and Navigation*, **152**, 3, 2005, pp. 195-205.

5. T. Lang and G. Hayes, "Exploitation of Bistatic Doppler Measurements in Multistatic Tracking," IEEE Conference on Information Fusion, 2007, pp. 1-8.

6. M. Petsios, E. Alivizatos, N. Uzunoglu, "Manoeuvring Target Tracking Using Multiple Bistatic Range and Range-Rate Measurements," *Signal Processing*, **87**, 4, 2007, pp. 665-686.

7. B. La Cour, Bayesian "Multistatic Tracking with Doppler-Sensitive Waveforms," Proceedings of the IEEE OCEANS Conference, 2007, pp. 1-6.

8. M. Chernaikov, *Bistatic Radar*, New York, Wiley, 2008.

9. J. C. Toomay and P. J. Hannen, *Radar Principles, Third Edition*, Norwich, NY, Scitech, 2004.

10. K. Kastella and C. Kreucher, "Multiple Model Nonlinear Filtering for Low Signal Ground Target Applications," *IEEE Transactions Aerospace and Electronic Systems*, **41**, 2, April 2005, pp. 549-564.

11. J. C. Strikwerda, *Finite Difference Schemes and Partial Differential Equations*, New York, Chapman and Hall, 1989.

12. C. Kreucher, B. Shapo, and R. Bethel, "Multitarget Detection and Tracking using Multi-sensor Passive Acoustic Data," Proceedings of the IEEE Aerospace Conference, 2009, pp. 1-16.

Introducing the Authors

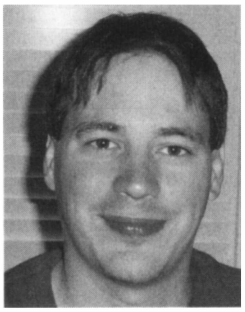

Dr. Christopher M. Kreucher received the BS, MS, and PhD in Electrical Engineering from the University of Michigan in 1997, 1998, and 2005, respectively. He is currently a Principal System Engineer at Integrity Applications Incorporated in Ann Arbor, Michigan. From 1998 to 2008, he was a Staff Scientist at General Dynamics Advanced Information Systems' Michigan Research & Development Facility (formerly, ERIM). His current research interests include nonlinear filtering, Bayesian multi-target tracking, and using information-theoretic methods for optimal sensor utilization.

Solicitation for Measurements Corner

We welcome contributions for future installments of the Measurements Corner. Please send them to Brian Fischer and Ivan LaHaie, and they will be considered for publication as quickly as possible. Contributions can range from short notes to full-length papers on all topics related to RF measurement technology and its applications, including antennas, propagation, materials, scattering, and radar cross section. New or unique measurement techniques are of particular interest.